Laser and Particle Beams (2000), *18*, 275–289. Printed in the USA.

Line shape modeling of multielectron ions in plasmas

P.A. LOBODA, I.A. LITVINENKO, G.V. BAYDIN, V.V. POPOVA, and S.V. KOLTCHUGIN

Russian Federal Nuclear Center—All Russian Institute of Technical Physics (RFNC VNITF) P.O. Box 245, Snezhinsk, Chelyabinsk region, 456770, Russia

(Received 14 June 1999; Accepted 14 June 1999)

Abstract

A density-matrix theoretical model to calculate spectral line profiles of general multielectron ions in plasmas is described. The line-profile calculation involves electron collisional and radiative relaxation of ionic states, the emitter's motion (Doppler effect) and its interaction with a quasi-static ion microfield. Using the LineDM computer package implementing this model, line-profile calculations of the *K*- and *L*-shell transitions in Al XII, Ar XVII, Ar XVI, Cu XX, and Xe XLV ions have been performed in the context of plasma diagnostic issues of recent laboratory experiments. Comparisons of the calculated line profiles with experimental and other theoretical data show the applicability of the model and package for the detailed computational analysis of line radiation spectra from multielectron emitters in hot dense plasmas.

1. INTRODUCTION

In recent years, experimental and theoretical studies of line radiation spectra from high-*Z* emitters in high-temperature laboratory plasmas have largely been stimulated by the intensive investigations into the problems of inertial confinement fusion (ICF) and the development of high-brightness table-top sources of X-ray radiation. A detailed theoretical description of X-ray transition line profiles of high-*Z* ions is of particular interest for diagnosing and probing hot, dense laboratory plasmas (Yaakobi *et al.*, 1979; Hauer, 1981; Moreno *et al.*, 1993; Keane *et al.*, 1994*a*; Hammel *et al.*, 1994; Mancini *et al.*, 1996), appropriate treatment of line radiation transfer (Iglesias *et al.*, 1987; Olson *et al.*, 1994; Mancini *et al.*, 1994), and evaluation of potential laser gains in various laboratory X-ray laser schemes (Derzhiev *et al.*, 1986; Griem, 1986; Moreno *et al.*, 1989; Elton, 1990; Calisti *et al.*, 1990; Lykov *et al.*, 1992; Loboda *et al.*, 1992, 1993, 1997).

Until recently, line-profile studies were performed mostly for the simplest *K*-shell $n = 2 - 4 \rightarrow 1$ transitions in H- and He-like ions with $Z = 10 - 20$ as applied to X-ray diagnostics of laboratory plasmas (Yaakobi *et al.*, 1979; Hauer, 1981; Akhmedov *et al.*, 1985; Stamm *et al.*, 1987). In the last decade, owing to considerable improvement of experimental techniques of registering X-ray line radiation spectra (Skobelev *et al.*, 1995; Faenov *et al.*, 1996; Rosmej *et al.*, 1997) and the increasing capabilities of computing facilities, growing attention is being given to theoretical modeling of more complex line radiation spectra. This refers primarily to the lines of *K*-shell transitions from highly excited and autoionizing states, and transitions between the excited states as well as to the *L*-shell transitions in more complex ions (Woltz & Hooper, 1988; Calisti *et al.*, 1990; Mancini *et al.*, 1991, 1996; Lykov *et al.*, 1992; Loboda *et al.*, 1992, 1993; Hammel *et al.*, 1994; Keane *et al.*, 1994*a*,*b*).

The emitter's line profile in plasmas is formed under the effect of various broadening mechanisms. For high-*Z* ions, the main types of line broadening are those due to the electric microfields produced by plasma ions and electrons (Stark broadening), natural, and Doppler broadening (Baranger, 1962; Griem, 1974; Derzhiev *et al.*, 1986). Stark broadening due to plasma electrons is generally described by using the results of the nonadiabatic impact theory (Baranger, 1962; Grien, 1974), which is valid in the majority of cases of practical interest. Ion Stark broadening is most commonly considered in the quasi-static approximation (Griem, 1974) which neglects the motion of perturbing ions. This approximation implies that the typical fluctuation frequencies of plasma ion microfield at the emitter are much smaller than the average Stark line shifts produced by this microfield. Relevant estimates and calculations show that for a wide range of applications the quasi-static approximation can often be found valid and therefore is generally used in practical line profile calculations (Yaakobi *et al.*, 1979; Hauer *et al.*, 1981; Stamm *et al.*, 1987; Woltz & Hooper, 1988; Moreno *et al.*, 1989, 1993; Calisti *et al.*, 1990; Mancini *et al.*, 1991,

Address correspondence and reprint requests to: Presently, Senior Scientist at the Division of Theoretical Physics and Applied Mathematics, RFNC VNITF, P.O. Box 245, Snezhinsk, Chelyabinsk region, 456770, Russia. E-mail: p.a.loboda@vniitf.ru

1996; Lykov *et al.*, 1992; Loboda *et al.*, 1992, 1993, 1997; Hammel *et al.*, 1994; Keanse *et al.* 1994a,b).

However, even with the quasi-static approximation for plasma ions and impact approximation for electrons, the practical line-profile calculations for multielectron ions encounter significant computational difficulties. Therefore, appropriate numerical models have only recently been developed (Woltz & Hooper, 1988; Calisti *et al.*, 1990, 1994; Mancini *et al.*, 1991) with the advent of high-performance computers and the progress of sufficiently reliable and general-purpose methods of atomic data calculations (Froese Fischer, 1978; Cowan, 1981; Dyall *et al.*, 1989; Parpia *et al.*, 1992, 1996). The relevant line-profile models of Woltz & Hooper (1988) and Calisti *et al.* (1990) are based on the results of traditional line-broadening theory and involve the computation of the Fourier transform of the dipole autocorrelation function under the assumption that atomic density matrix is diagonal with respect to the emitter states (Baranger, 1962; Griem, 1974). This approach, however, gives no way to consider the main line-broadening mechanisms along with the effect of plasma ion microfields on the populations of the emitters' states that can appear to be important in the cases of Non-LTE distribution of populations and essential Stark mixing within the sets of the upper $\{\alpha\}$ or lower $\{\beta\}$ states corresponding to the transitions $\{\alpha\} \to \{\beta\}$ of interest. Specifically, such a situation may occur for the manifolds of doubly-excited upper states of *K*-, *L*-shell transitions (satellite transitions), which emission spectra can serve as a powerful diagnostic tool for probing the Non-LTE plasmas driven by ultrashort laser pulses (Mancini *et al.*, 1996; Osterheld, 1997; Elton *et al.*, 1997). Another example is given by the problem of evaluating small signal gain for the recombination and resonantly photopumped X-ray laser schemes on the $\{\alpha\} \to \{\beta\}$ transitions with different population inversion densities (Gasparyan *et al.*, 1994; Loboda *et al.*, 1997).

Apparently, the most consistent approach allowing us to account for the both effects simultaneously is to formulate the line-profile and spectral gain (absorption) calculation model within the framework of density matrix formalism (Zhidkov & Yakovlenko, 1985; Zhidkov *et al.*, 1986; Anufrienko *et al.*, 1990; Gasparyan *et al.*, 1994; Loboda *et al.*, 1997; Loboda & Popova, 1997).

In this paper, we describe a generalized model and the LineDM computer package to calculate line profiles for arbitrary multielectron ions in plasmas using the density matrix approach. This generalized model is an extension of previously developed approximate density-matrix model for the n to n' transitions of simple ions (H-, He-, Li-, and Na-like) implemented in the HELM code (Loboda *et al.*, 1992, 1997; Loboda & Popova, 1997) and is largely free of its limitations. We also present some examples of line-profile calculations for the *K*- and *L*-shell transitions of He-, Li-, and Ne-like ions done with the LineDM package as applied to some diagnostic issues of recent laser-plasma experiments.

2. MODEL FORMULATION

Line-profile calculations for high-*Z* emitters in plasmas using the density matrix approach are based on the solution of quantum kinetic equation for density matrix elements ρ of an emitter, interacting with plasma ion microfield and spontaneous radiation field or a probe plane electromagnetic wave with a frequency ω, close to the frequencies of transitions of interest. Considering the interaction with electromagnetic field V_μ as a small perturbation, the equation for density matrix ρ can be solved to the first-order approximation in V_μ (Rautian *et al.*, 1979):

$$\rho = \rho^0 + \rho^\mu,$$

$$[\partial/\partial t + \boldsymbol{v}_i\nabla]\rho^0 = -\frac{i}{\hbar}[H + V_F, \rho^0] + R\rho^0 + Q,$$

$$[\partial/\partial t + \boldsymbol{v}_i\nabla]\rho^\mu = -\frac{i}{\hbar}[H + V_F, \rho^\mu] + R\rho^\mu - \frac{i}{\hbar}[V_\mu, \rho^0]. \quad (1)$$

Here, $\boldsymbol{v}_i$ is a velocity of the emitter, ρ^μ is a small value induced by the quasi-resonant interaction V_μ of the emitter with the electromagnetic field mode μ, and H is the diagonal Hamiltonian matrix of the isolated emitter.

The perturbation V_F induced by an ion microfield $\boldsymbol{F}$ is described by the nondiagonal operator $V_F = -\boldsymbol{dF}$, where $\boldsymbol{d}$ is the emitter dipole operator. In high-temperature multicharged ion (MCI) plasmas, typical perturbation values V_F for upper and lower states $\{\alpha_0\}$ and $\{\beta_0\}$ of spectrally resolved X-ray lines $\{\alpha_0\} \to \{\beta_0\}$ are essentially less than the transition energies $E_{\alpha\beta}$. Therefore, the states $\{\alpha_0\}$ and $\{\beta_0\}$ are mixed by plasma ion microfield only with the closely spaced states $\{\alpha'\}$ and $\{\beta'\}$, $|E_{\alpha_0\alpha'}|, |E_{\beta_0\beta'}| \ll E_{\alpha_0\beta_0}$, thus comprising the sets of states $\{\alpha\} = \{\alpha_0\} \otimes \{\alpha'\}$ and $\{\beta\} = \{\beta_0\} \otimes \{\beta'\}$ relevant to the perturbed-transition line profile $\{\alpha\} \to \{\beta\}$ of interest. The states $i = \alpha, \beta$ of the emitter are specified as $i \equiv |\gamma_i P_i J_i M_i\rangle$ where $P_i = \pm 1$ is the parity, J_i and $M_i = (J_i)_z$ are angular momentum quantum numbers, and γ_i represents a set of all other quantum numbers.

The operator $R = R_c + R_r + R_a$ responsible for ion-state relaxation due to electron collisional (R_c), radiative (R_r) and autoionizing (R_a) transitions is a tetradic, or four-index operator in the Liouville space, with the elements

$$(R\rho)_{ab} = \sum_{a'b'} R_{ab}^{a'b'}\rho_{a'b'}, \quad (2)$$

where a, b, a', b' denote the emitter states.

Diagonal source operator Q represents the external (recombination-ionization) feeding of the emitter states.

The elements of the radiative relaxation operator in Eq. (1) can be represented as the sum of two elements:

$$(R_r)_{ab}^{a'b'} = (R_r^{(1)})_{ab}^{a'b'} + (R_r^{(2)})_{ab}^{a'b'}, \quad (3)$$

https://doi.org/10.1017/S0263034600182175 Published online by Cambridge University Press

comprising the matrices of radiative depletion $\boldsymbol{R}_r^{(1)}$ and radiative feeding $\boldsymbol{R}_r^{(2)}$ of the emitter states (Mollow, 1977; Zhidkov & Yakovlenko, 1985; Loboda *et al.*, 1997; Loboda & Popova, 1997):

$$\begin{aligned}(R_r^{(1)})_{ab}^{a'b'} &= \mathrm{Re}\{(R_r^{(1)})_{ab}^{a'b'}\} \\ &= -\tfrac{1}{2}\{(\mathcal{D}^+\mathcal{D})_{aa'}\delta_{b'b} + (\mathcal{D}^+\mathcal{D})_{b'b}\delta_{aa'}\} \\ &\quad + (R_r^{ph})_{ab}^{ab}\delta_{aa'}\delta_{b'b}, \\ (R_r^{(2)})_{ab}^{a'b'} &= \mathcal{D}_{aa'}\mathcal{D}_{b'b}^{+} \end{aligned} \tag{4}$$

where the transition operators $\mathcal{D}$ describe both spontaneous and stimulated radiative transitions driven by an external radiation field with photon modal densities $\bar{n}_\omega$ (Loboda *et al.*, 1997):

$$\mathcal{D} = \sum_{a,b}\left(\frac{4|\omega_{ab}|^3}{3\hbar c^3}\right)^{1/2}\boldsymbol{d}_{ba}\sqrt{\bar{n}_{|\omega_{ab}|} + \theta(\omega_{ab})}|b\rangle\langle a|. \tag{5}$$

Here, $\boldsymbol{d}_{ba}$ and $\omega_{ab} = (E_a - E_b)/\hbar$ are the dipole matrix element and the frequency of the transition $a \to b$ between the states a and b with the energies $E_{a,b}$; $\theta(\omega_{ab})$ is the step function: $\theta(\omega_{ab} < 0) = 0$, $\theta(\omega_{ab} > 0) = 1$. Photoionizing contribution to radiative relaxation in Eq. (4) is included through the diagonal terms

$$(R_r^{ph})_{ab}^{ab} = -\tfrac{1}{2}(\Gamma_a^{ph} + \Gamma_b^{ph}), \tag{6}$$

where $\Gamma_a^{ph}, \Gamma_b^{ph}$ represent the total photo-ionization rates of the ionic states a, b. Therefore, the diagonal elements $(R_r^{(1)})_{ab}^{ab}$ comprise the radiative widths Γ_{ab}^r of the $a - b$ transition lines:

$$\begin{aligned}(R_r^{(1)})_{ab}^{ab} &= -\Gamma_{ab}^r/2 = -\tfrac{1}{2}(\Gamma_a^r + \Gamma_b^r), \\ \Gamma_i^r \equiv \Gamma_{ii}^r &= -(R_r)_{ii}^{ii} \quad (i = a, b), \end{aligned} \tag{7}$$

where $\Gamma_i^r (i = a, b)$ specifies the radiative widths of the states a, b. The elements $(R_r^{(2)})_{ab}^{a'b'}$ in Eq. (4) are responsible for radiative feeding of the states $b = a$ from the states $a' = b'$ with the rates $(R_r^{(2)})_{aa}^{b'b'} = |\mathcal{D}_{ab'}|^2 > 0$, $b' \neq a$, as well as the interference coupling of $\{a \neq a'\}$ and $\{b \neq b'\}$ states driven by the radiative relaxation.

The imaginary part of the radiative relaxation operator $\mathrm{Im}\{R_r^{(1)}\rho\}$ responsible for radiative (Lamb) shifts (see, e.g., Mollow & Miller, 1969), is included in H, assuming radiative corrections to be incorporated into the calculation of the energy spectrum of an isolated ion.

The relaxation of ionic states under the effect of binary electron collisions can be appropriately described with a general expression for the elements of collisional operator R_c obtained in relaxation theory by Smith & Hooper (1967). Including the contribution to R_c due to collisional transitions to the nearby ionization stages, R_c^i, in the similar way as for the radiative relaxation in Eq. (4) and using the impact approximation within the frequency range of interest ($\Delta\omega_{pq} = \omega - \omega_{pq} \to 0$, see Baranger, 1962; Cooper, 1967) one obtains:

$$\begin{aligned}(R_c)_{ab}^{a'b'} &= -\frac{8e^4a_0^2}{3\hbar^2}N_e\left(\frac{\pi m}{2T_e}\right)^{1/2} \\ &\quad \times \left\{\sum_c [\delta_{bb'}\boldsymbol{d}_{ac}\boldsymbol{d}_{ca'}G_{aca'}^{cb} + \delta_{aa'}\boldsymbol{d}_{b'c}\boldsymbol{d}_{cb}G_{b'cb}^{ac}]\right. \\ &\quad \left. - \boldsymbol{d}_{aa'}\boldsymbol{d}_{b'b}[G_{ab'a'b}^{ab'} + G_{a'bab'}^{a'b}]\right\} \\ &\quad + (R_c^i)_{ab}^{ab}\delta_{aa'}\delta_{b'b}. \end{aligned} \tag{8}$$

Here, N_e and T_e are plasma electron density and temperature, respectively, $G_{ijk(l)}(\Delta\omega_{pq} = 0)$ is a function describing binary electron-ion collisions in the impact approximation. Other notations are conventional. Diagonal elements $(R_c^i)_{ab}^{ab}$ have the form similar to Eq. (6):

$$(R_c^i)_{ab}^{ab} = -\tfrac{1}{2}(\Gamma_a^{ci} + \Gamma_b^{ci}), \tag{9}$$

where $\Gamma_a^{ci}, \Gamma_b^{ci}$ represent the sums of total rates of collisional ionization, radiative, three-body, and dielectronic recombination from the states a, b.

From the Eqs. (4) and (8) one can readily see that the structure of the collisional operator R_c is similar to that of radiative relaxation operator R_r. It is the fundamental consequence of the fact that radiative and impact-collisional relaxations are both described in the unified form using the scattering T-matrix representation (Zhidkov & Yakovlenko, 1985). The third term in the brackets in Eq. (8) describes collisional feeding of the states $b = a$ from the states $a' = b'$ in the dipole approximation with the rates

$$(R_c)_{aa}^{b'b'} = \frac{16e^4a_0^2}{3\hbar^2}N_e\left(\frac{\pi m}{2T_e}\right)^{1/2}|\boldsymbol{d}_{ab'}|^2G_{ab'b'a}^{ab'}, \tag{10}$$

as well as the interference coupling of $\{a \neq a'\}$ and $\{b \neq b'\}$ states caused by electron collisions. This term vanishes for the diagonal elements $(R_c)_{ab}^{ab}$ that are responsible for the collisional width and shift Γ_{ab}^c and Δ_{ab}^c of the isolated line $a - b$, and may be expressed in the form (Cooper, 1967):

$$\begin{aligned}(R_c)_{ab}^{ab} &= -\Gamma_{ab}^c/2 - i\Delta_{ab}^c, \ \Gamma_{ab}^c = \Gamma_a^c + \Gamma_b^c, \\ \Gamma_i^c \equiv \Gamma_{ii}^c &= -\mathrm{Re}\{(R_c)_{ii}^{ii}\} \quad (i = a, b), \end{aligned} \tag{11}$$

where $\Gamma_i^c (i = a, b)$ specifies the collisional widths of the states a, b. The influence of the collisional shift Δ_{ab}^c is generally rather small due to cancellation of partial contributions of different sign from the perturbing states (Griem,

https://doi.org/10.1017/S0263034600182175 Published online by Cambridge University Press

1974; Vainshtein, *et al.* 1979). Moreover, in the MCI-plasmas, electron collisional broadening is rarely found dominant, therefore the line collisional shifts are usually omitted (Woltz & Hooper, 1988; Calisti *et al.*, 1990) or treated approximately (Griem, 1974). In the present model, electron collisional shifts of line components are not included.

If the transitions of interest $\{\alpha\} \to \{\beta\}$ also involve autoionizing states, the relevant elements of relaxation operator R_a, are evaluated similarly to Eq. (8) with $\Gamma_{a,b}^{ph}$ substituted by the total autoionization widths $\Gamma_{a,b}^{Auto}$ of ionic states a, b.

Collisional relaxation, governed by Eq. (8), is conveniently expressed as the sum of two contributions responsible for the transitions within the sets of closely-spaced states $\{\alpha\}$ or $\{\beta\}(R_c^{(1)})$ and transitions to all other states of the emitter, including continuum states $(R_c^{(2)})$. The difference between these contributions is governed by their G-functions (see Appendix).

Thus, Eq. (1) provided the necessary information on the state populations and radiative properties of the emitter within the spectral range of transitions $\{\alpha\} - \{\beta\}$ at some values of ion microfield $\boldsymbol{F}$ and ion velocity $\boldsymbol{v}$. The state populations are described by the diagonal elements of density matrix ρ^0 (ρ^0 is normalized to the number density of the emitters, cm^{-3}), while the line profile and spectral gain (absorption) at the transitions $\{\alpha\} - \{\beta\}$ are governed by the frequency dependence of reduced nondiagonal elements of density matrix $\rho_{\alpha\beta}^{\mu}(\omega)$, free of explicit dependence on resonant exponential factor of electromagnetic field: $\rho_{\alpha\beta}^{\mu} = \rho_{\alpha\beta}^{\mu}(\omega) \cdot \exp[-i(\omega t - \boldsymbol{kr})]$ (Rautian *et al.*, 1979).

The problem considered will next be treated in the local formulation for the quasi-stationary conditions (Derzhiev *et al.*, 1986) under the assumption of quasi-static ion broadening. Therefore, the equations for the elements ρ^0 in Eq. (1) become algebraic ones. Moreover, the diagonality of the quasi-static field perturbation matrix $V_F = -d_z F, F = F_z$, in magnetic quantum numbers $M = J_z$ (the z-axis is chosen to be in the direction of $\boldsymbol{F}$) and the symmetry properties of the relaxation operator elements result in the fact that the ρ^0 matrix is also diagonal in M (Gasparyan *et al.*, 1994; Loboda & Popova, 1997). This enables one to remove the explicit dependence of the equations for the elements $\rho_{\alpha\beta}^{\mu}(\omega)$ on the vector components of the electromagnetic field, coming from V_μ through the dipole-interaction scalar products, by writing

$$\rho_{\alpha\beta}^{\mu}(\omega) = \sum_q C_q^{\mu^*} \rho_{\alpha\beta}^{q}(\omega) \delta_{q, M_\alpha - M_\beta}, \ \alpha \in \{\alpha\}, \beta \in \{\beta\}, \quad (12)$$

where the spherical tensor components $C_q^{\mu}, (q = 0, \pm 1)$ are proportional to the amplitude and the polarization vector q-component e_q^{μ} of the electromagnetic field mode μ (Loboda *et al.*, 1997).

For the emitter interaction with a plane electromagnetic wave (absorption and stimulated emission), the equations for the elements $\rho_{\alpha\beta}^{q}(\omega)$ are reduced to the form

$$\begin{aligned}
&\rho_{\alpha\beta}^{\mu}(\omega)[i(\omega - \omega_{\alpha\beta} - \boldsymbol{kv}_i) - \Gamma_{\alpha\beta}] \\
&\quad + \sum_{\alpha'\beta'}{}' R_{\alpha\beta}^{\alpha'\beta'} \rho_{\alpha'\beta'}^{\mu}(\omega) \\
&\quad - \frac{i}{\hbar} \sum_{\alpha'\beta'} [(V_F)_{\alpha\alpha'} \rho_{\alpha'\beta}^{q}(\omega) - \rho_{\alpha\beta'}^{q}(\omega)(V_F)_{\beta'\beta}] \\
&= \frac{i}{\hbar} \sum_{\alpha'\beta'} [\rho_{\alpha\alpha'}^0 (d_q)_{\alpha'\beta} - (d_q)_{\alpha\beta'} \rho_{\beta'\beta}^0], \qquad (13)
\end{aligned}$$

where the elements $\rho_{\alpha\alpha'}^0$ are found from the equations:

$$\begin{aligned}
&\rho_{\alpha\alpha'}^0 (i\omega_{\alpha\alpha'} + \Gamma_{\alpha\alpha'}) - \sum_{\substack{aa' \\ a, a' \in \{\alpha\}}}{}' [(R_c^{(1)})_{\alpha\alpha'}^{aa'} + (R_r^{(1)})_{\alpha\alpha'}^{aa'}] \rho_{aa'}^0 \\
&\quad - \sum_{\substack{cc' \\ c, c' \notin \{\alpha\}}}{}' [(R_c^{(2)})_{\alpha\alpha'}^{cc'} + (R_r^{(2)})_{\alpha\alpha'}^{cc'}] \rho_{cc'}^0 \\
&\quad + \frac{i}{\hbar} \sum_{a \in \{\alpha\}} [(V_F)_{\alpha a} \rho_{a\alpha'}^0 - \rho_{\alpha a}^0 (V_F)_{a\alpha'}] = Q_{\alpha\alpha'} \delta_{\alpha\alpha'} \qquad (14)
\end{aligned}$$

(similar for $\rho_{\beta\beta'}^0$), where the radiative transitions between the closely-spaced states are neglected due to their minor values. It is also supposed for Eqs. (13) and (14), that the upper and lower states coupled by the radiative-collisional transitions are not mixed by ion microfield, that is, the elements like $(V_F)_{\alpha\beta}$ are vanishingly small.

The interaction with spontaneous emission field is described by the analogous equations with the right-hand side of Eqs. (14) substituted by (Loboda & Popova, 1997):

$$\sum_{\alpha'} \rho_{\alpha\alpha'}^0 (d_q)_{\alpha'\beta}. \qquad (15)$$

Equation (14) formulates the local quasi-stationary kinetic model of emitter state populations in the density matrix approach. It can easily be shown, that nondiagonal elements ρ_{ab}^0 in Eq. (14) should be considered only for the non-LTE-populated states $a \neq b$ well-mixed by the plasma ion microfield. Contribution of the other states is described only by the diagonal elements ρ_{aa}^0, ρ_{bb}^0, that is populations, calculated in the framework of the traditional collisional-radiative (CR) model. Using the similar formulation, the problem of spectral gain calculation accounting for the ion microfield effect on the emitter-state populations was solved previously for the model case of the $n = 4$ to 3 and $n = 3$ to 2 transitions of H-like Ni XXVIII (Gasparyan *et al.*, 1994). We have implemented another variant to solve this problem (Loboda *et al.*, 1997): using a "dressed" basis of Stark states, reducing the perturbed Hamiltonian matrix $H + V_F$ to the diagonal form, an open system of the upper and lower Stark states $\{\alpha\} \otimes \{\beta\}$, coupled with radiative-collisional transitions $\{\alpha\} \rightleftarrows \{\beta\}$, was considered, where the contribution of the other ionic states was described with the effective source terms $\tilde{Q}_a, \tilde{Q}_\beta$ and depletion rates

https://doi.org/10.1017/S0263034600182175 Published online by Cambridge University Press

$\tilde{\Gamma}_\alpha, \tilde{\Gamma}_\beta$ from the CR-model calculations (Politov *et al.*, 1992). However, owing to inconsistencies in the atomic models employed and, thus, the need of special-purpose processing of CR-model calculated data, further practical development of this approach within the framework of the generalized density-matrix kinetic model has encountered unreasonable difficulties. Therefore at the moment, the local quasi-stationary model described by Eq. (18) is being implemented to consistently calculate microfield-affected populations of emitter states.

Simultaneous solution of the sets of Eqs. (13), (14) or (14), (15) enables us to obtain the spectral gain (absorption) profile $G(\omega)$ for the emitter lines formed by the $\{\alpha\} - \{\beta\}$ transition manifolds:

$$G(\omega) = \frac{4\pi\omega}{3c} \cdot \mathrm{Re} \left\langle i \sum_{\alpha\beta} (d_q)^*_{\alpha\beta} \rho^q_{\alpha\beta}(\omega) \right\rangle_{v_i, F}, \tag{16}$$

or spectral function $S(\omega)$

$$S(\omega) = \frac{I(\omega)}{I_\infty}, \quad I_\infty = \int_0^\infty I(\omega) d\omega, \tag{17}$$

specifying the line profile of spontaneous emission, where

$$I(\omega) = -\frac{4\omega^4}{3\pi c^3} \cdot \mathrm{Re} \left\langle \sum_{\alpha\beta, q} (d_q)^*_{\alpha\beta} \rho^q_{\alpha\beta}(\omega) \right\rangle_{v_i, F} \tag{18}$$

is the spectral power of spontaneous emission summed over the polarization $\mu = 1,2$ (Loboda & Popova, 1997).

If one neglects the variations in the factor ω^4 throughout the $\{\alpha\} - \{\beta\}$ line according to the quasi-resonant approximation, spectral function of spontaneous emission line can be expressed as follows [cf. Rautian *et al.* (1979) and Anufrienko *et al.* (1990)]:

$$S(\omega) = \frac{I(\omega)}{I_\infty}$$

$$= -\frac{1}{\pi} \frac{\mathrm{Re} \left\langle \sum_{\alpha\beta, q} (d_q)^*_{\alpha\beta} \rho^q_{\alpha\beta}(\omega) \right\rangle_{v_i, F}}{\sum_{\alpha, \gamma_\beta J_\beta} \frac{|\langle \gamma_\beta P_\beta J_\beta \| d \| \gamma_\alpha P_\alpha J_\alpha \rangle|^2}{2J_\alpha + 1} \langle \rho^0_{\alpha\alpha}(F) \rangle_F}. \tag{19}$$

Here, the notation $\langle \ldots \rangle_{v_i, F} \equiv \int_{-\infty}^{+\infty} f(v_i) dv_i \int_0^\infty W(F) dF$ denotes the averaging over the distributions $f(v_i)$ and $W(F)$ of the emitter velocities and ion microfields (Griem, 1974) and $\langle \gamma_\beta P_\beta J_\beta \| d \| \gamma_\alpha P_\alpha J_\alpha \rangle$ represents reduced matrix element of a dipole transition $\alpha - \beta$.

In high-temperature laboratory plasmas, high-Z emitter velocity distribution can always be considered as the Maxwellian one:

$$f(v_i) dv_i = \frac{1}{\sqrt{\pi}} \exp[-(v_i / v_{i0})^2] d(v_i / v_{i0}),$$

where $v_{i0} = \sqrt{2T_i / m_i}$ is the average thermal velocity of the emitter with the mass m_i at an ion temperature T_i.

For the line-profile model considered, a modified two-temperature Hooper model (Akhmedov *et al.*, 1985; Loboda & Popova, 1997), consistently allowing for the Coulomb electron-ion interactions in plasmas, will be employed to evaluate ion microfield distribution function $W(F)$ in Eqs. (16)–(19).

3. ATOMIC DATA

High-Z ions are typically featured by the multilevel energy spectra of the excited states stemming from the significant contribution of the relativistic and correlation effects (Cowan, 1981). Therefore, the calculation of high-Z emitter line profile should generally start from the construction of appropriate atomic model, that is, the consistent set of atomic data calculated to a required accuracy. Apparently, the most versatile tool to calculate atomic data for high-Z multielectron ions is offered by the multiconfigurational Dirac-Fock method (Dyall et al., 1989). Using this method, effective numerical algorithms were created, which, in particular, were implemented in the most up-to-date GRASP and GRASP^2 codes of Dyall *et al.* (1989) and Parpia *et al.* (1992, 1996). These codes are able to calculate atomic energy levels $E_{\gamma PJ}$ and radiative properties of multipole transitions with reasonably good accuracy and thus are employed to construct the atomic models for the line-profile calculations.

Using these codes, it is also possible to infer the equivalent values of reduced dipole-transition matrix elements (in atomic units, a.u.):

$$\langle \gamma_\beta P_\beta J_\beta \| d \| \gamma_\alpha P_\alpha J_\alpha \rangle$$

$$= \sqrt{\frac{\pi c (2J_\beta + 1)}{2E^3_{\alpha\beta}}}$$

$$\times \langle \gamma_\beta P_\beta J_\beta \| O^{(1)} \| \gamma_\alpha P_\alpha J_\alpha \rangle, \; E_\alpha > E_\beta. \tag{20}$$

Here, $c = 137.036$ is the speed of light (in a.u.), $\langle \gamma_\beta P_\beta J_\beta \| O^{(1)} \| \gamma_\alpha P_\alpha J_\alpha \rangle$ represents the reduced matrix element of multipole transition operator (Dyall *et al.*, 1989) for dipole radiation ($L = 1$), taken in the gauge corresponding to the relativistic length form. These values are calculated in the codes developed by Dyall *et al.* (1989) and Parpia *et al.* (1992, 1996) to obtain the oscillator strengths and radiative transition probabilities.

Matrix elements of the dipole operator component $d_q (q = 0, \pm 1)$ are given by the Wigner–Eckart theorem (Cowan, 1981):

$$(d_q)_{\alpha\beta} = (-1)^{J_\alpha - M_\alpha} \begin{pmatrix} J_\alpha & 1 & J_\beta \\ -M_\alpha & q & M_\beta \end{pmatrix}$$

$$\cdot \langle \gamma_\alpha P_\alpha J_\alpha \| d \| \gamma_\beta P_\beta J_\beta \rangle, \tag{21}$$

https://doi.org/10.1017/S0263034600182175 Published online by Cambridge University Press

where $\begin{pmatrix} J_\alpha & 1 & J_\beta \\ -M_\alpha & q & M_\beta \end{pmatrix}$ is the 3-j symbol, which is nonzero only for $q = M_\alpha - M_\beta$. From the general symmetry properties of matrix elements of irreducible tensor operators (Cowan, 1981; Karazija, 1987), it follows that

$$(d_q)^*_{\alpha\beta} = (-1)^q (d_{-q})_{\beta\alpha}$$

$$\langle \gamma_\beta P_\beta J_\beta \| d \| \gamma_\alpha P_\alpha J_\alpha \rangle = (-1)^{J_\beta - J_\alpha} \langle \gamma_\alpha P_\alpha J_\alpha \| d \| \gamma_\beta P_\beta J_\beta \rangle. \quad (22)$$

By using Eqs. (21), (22) along with the orthogonality and summation properties of 3-j symbols (Cowan, 1981; Karazija, 1987), the summation over the intermediate M-states in Eqs. (4) and (8) is reduced to the summation over the energy levels:

$$\begin{aligned}
(\boldsymbol{\mathcal{D}}^+\boldsymbol{\mathcal{D}})_{aa'} &= \sum_c \boldsymbol{\mathcal{D}}^+_{ac}\boldsymbol{\mathcal{D}}_{ca'} \\
&\cong \frac{4}{3\hbar c^3}[J_a]^{-1}\delta_{J_a,J_{a'}}\delta_{M_a,M_{a'}}\delta_{P_a,P_{a'}} \\
&\times \sum_{\gamma_c J_c} |\omega_{ac}|^3 [\bar{n}_{|\omega_{ac}|} + \theta(\omega_{ac})] \\
&\times \langle \gamma_c P_c J_c \| d \| \gamma_a P_a J_a \rangle \\
&\times \langle \gamma_c P_c J_c \| d \| \gamma_{a'} P_{a'} J_{a'} \rangle \\
\sum_c \boldsymbol{d}_{ac}\boldsymbol{d}_{ca'} G^{cb}_{aca'} &= [J_a]^{-1}\delta_{J_a,J_{a'}}\delta_{M_a,M_{a'}}\delta_{P_a,P_{a'}} \\
&\times \sum_{\gamma_c J_c} \langle \gamma_c P_c J_c \| d \| \gamma_a P_a J_a \rangle \\
&\times \langle \gamma_c P_c J_c \| d \| \gamma_{a'} P_{a'} J_{a'} \rangle \cdot G^{cb}_{aca'}, \qquad (23)
\end{aligned}$$

where $[J_a] \equiv (2J_a + 1)$. It is also assumed, that the states a and a' (b and b') have close energies, since only these states actually enter into the relevant components of the relaxation operator. The remaining terms, describing radiative-collisional feeding, are nondiagonal in M and provide the symmetry property of the elements of radiative-collisional relaxation operator $R^{a'b'}_{ab}$ relative to q:

$$q = M_a - M_b = q' = M_{a'} - M_{b'}. \quad (24)$$

This relation formally provides the above mentioned M-diagonal property of the ρ^0 elements and significantly simplifies the coefficient matrices for the ρ^q in Eqs. (13) and (15).

Using the irreducible-component representation for density matrix (Blum, 1981), one easily shows that the density-matrix elements obey the following symmetry relations:

$$\begin{aligned}
&\langle \gamma_a P_a J_a - M_a | \rho^0 | \gamma_a P_a J_a - M_a \rangle \\
&\quad = \langle \gamma_a P_a J_a M_a | \rho^0 | \gamma_a P_a J_a M_a \rangle \\
&\langle \gamma_a P_a J_a - M_a | \rho^{-q} | \gamma_b P_b J_b - M_b \rangle \\
&\quad = (-1)^{J_a - J_b} P_a P_b \\
&\quad \cdot \langle \gamma_a P_a J_a M_a | \rho^q | \gamma_b P_b J_b M_b \rangle. \qquad (25)
\end{aligned}$$

Coupled with the general symmetry property of density-matrix elements,

$$\rho^*_{ab} = \rho_{ba}, \quad (26)$$

these symmetry relations essentially reduce rank of matrices in Eqs. (13)–(15).

4. NUMERICAL IMPLEMENTATION OF THE MODEL

Theoretical model, described in the previous section, was implemented in the numerical model and the computer package LineDM. The package includes special-purpose programs of input data generation and processing, a code to calculate ion microfield distribution function, and the main computation module that evaluates density-matrix elements $\rho^q_{\alpha\beta}(\omega), \rho^0_{\alpha\alpha}(\rho^0_{\beta\beta})$ and performs necessary integrations and convolutions to obtain the spectral distributions in Eqs. (16)–(19) of interest. The LineDM code also incorporates a special-purpose module for the less-square-fit comparisons of the calculated line profiles and experimental spectra with smoothing the experimental spectra over the given number of adjacent points, if necessary. The set of algebraic linear Eqs. (13)–(15) in complex variables are solved by using elimination technique with the selection of principal element.

To solve the particular problem, the following input data are to be specified.

- Frequency range $[\omega_{\min}, \omega_{\max}]$, in which the spectral distributions are calculated. The step of frequency grid, is generally nonuniform and is adjusted as the calculation proceeds to reliably represent the $S(\omega), G(\omega)$ functions in the ranges of spectral features.
- Atomic number Z_A and weight A of the emitter and its spectroscopic symbol z.
- Plasma parameters: mass density ρ [g/cm^2], ion and electron temperatures T_i, T_e [keV]; ionization balance, defined by the set of Coulomb charges, atomic weights and relative abundances of plasma ions $Z_i, A_i, C_i, \sum_i^k C_i = 1$ (k is the number of ionic species).
- The set of energy levels E_j (a.u.), their degeneracies $g_j = [J_j]$, parities P_j, principal quantum numbers of valent electrons, partial relaxation widths due to ionization-recombination processes (if necessary), and array of reduced dipole-transition matrix elements between these levels $\langle j' \| d \| j \rangle$.

https://doi.org/10.1017/S0263034600182175 Published online by Cambridge University Press

If for the states of interest non-LTE population distribution occurs and kinetic effects due to ion microfield are vanishingly small (or neglected), input data of line profile and spectral gain calculations also involve level populations $N(\gamma_\alpha P_\alpha J_\alpha)[N(\gamma_\beta P_\beta J_\beta)]$ from the CR-model calculations. Here, Eq. (14) for the elements ρ^0 are not solved, and the populations of M-states $\{\alpha\}(\{\beta\})$ in Eqs. (13) and (15) are just defined as

$$\rho^0_{\alpha\alpha} = \delta_{\alpha\alpha'} N(\gamma_\alpha P_\alpha J_\alpha)/g_\alpha. \tag{27}$$

When it is essential to allow for radiative transitions driven by an external radiation field, photon modal densities $\bar{n}_\omega$ of the relevant radiation source are also specified.

Sets of the upper and lower levels $\{\alpha\} = \{\alpha_0\} \otimes \{\alpha'\}$ and $\{\beta\} = \{\beta_0\} \otimes \{\beta'\}$, involved in the transitions of interest, are formed in every specific case depending on the frequency interval and plasma density considered. This is done first by using the condition that the energies $E_{\alpha_0\beta_0}$ of radiative transitions $\alpha_0 - \beta_0$ fall within the interval $[E_{\min}, E_{\max}]$ and then expanding these sets $\{\alpha_0\},\{\beta_0\}$ to include all other closely-spaced states $\{\alpha'\},\{\beta'\}$ well-coupled by plasma ion microfield either to $\{\alpha_0\},\{\beta_0\}$ or to themselves:

$$(\bar{V}_F)_{\alpha_0\alpha'}/|E_{\alpha_0\alpha'}| \geq \delta_\alpha,$$

$$(\bar{V}_F)_{\tilde{\alpha}'\alpha'}/|E_{\tilde{\alpha}'\alpha'}| \geq \delta_\alpha,\ \tilde{\alpha}', \alpha' \in \{\alpha'\} \tag{28}$$

(same for the lower β-levels). Here, the coupling parameters $\delta_\alpha(\delta_\beta)$ control the inclusion of ion-microfield effect among the upper (lower) levels, and

$$(\bar{V}_F)_{\alpha_0\alpha'} = \left(\frac{\langle\gamma_{\alpha_0} P_{\alpha_0} J_{\alpha_0}\|d\|\gamma_{\alpha'} P_{\alpha'} J_{\alpha'}\rangle}{3\cdot g_{\alpha_0}}\right)^{1/2} \times F_0,$$

$$F_0 = 0.52\cdot(\langle Z^{3/2}\rangle)^{2/3}(\rho/\langle A\rangle)^{2/3} \tag{29}$$

(in a.u.) represents a characteristic value of interaction with the Holtzmark ion microfield F_0.

By now, a substantial set of line-profile calculations for the K, L-shell transitions of H-, He-, Li-, Ne-, and Na-like Al, Mg, Ar, Cu, and Xe has been performed using the LineDM package in the context of plasma diagnostic issues in recent laboratory experiments (Hammel *et al.*, 1994; Keane *et al.*, 1994b, Bollanti *et al.*, 1995; Faenov *et al.*, 1996; Faenov, 1998; Stepanov *et al.*, 1998; Osterheld, 1998). Some results of these calculations are presented below.

5. SOME RESULTS AND DISCUSSION

Currently, X-ray spectroscopy has already become a traditional tool of diagnosing the parameters of high-temperature laboratory and astrophysical plasmas. The methods of X-ray spectroscopic diagnostics are based on fitting of the observable characteristics of calculated and experimental line radiation spectra from high-Z emitters in plasmas registered with various dispersive elements (flat and bent crystals or gratings).

Due to significant improvement of resolution and luminosity of crystal spectrographs achieved during the last decade, the methods of plasma density and temperature diagnostics using the lineshapes and intensity ratios of high-Z ion spectral lines have found a wide utility in the present-day laboratory experiments. Specifically, the evaluation of the ICF plasma parameters is usually inferred from the fitting of calculated and experimental line radiation spectra from diagnostic dopants seeded into the shell or fuel regions of laser targets. To probe the plasmas of electron densities $N_e \simeq 10^{22}$–10^{24} cm^{-3}, the fuel region of ICF capsules is typically doped with a small abundance of Ne or Ar. In this connection, primary emphasis is centered on the K_β-shell emission lines of H-, He-, and Li-like ions since these lines, as a rule, are found to be optically thin and susceptible to the sufficient Stark broadening, while the emitters themselves have rather simple atomic structure.

Specifically, line profiles of Ar He$_\beta$ ($1s3l - 1s^2$) and its dielectronic K_β-satellites $1snl3l' - 1s^2nl$ ($n = 2,3$), located at the long-wavelength side of the Ar He$_\beta$ line, were registered in the NOVA-laser experiments with indirectly driven DD-filled capsules doped with a trace abundance of Ar. Analysis of the experimental data has shown that the account of the contribution due to satellite lines at moderate plasma temperatures $T \leq 1$ keV allows us to avoid an overestimation of plasma densities inferred with the Ar He$_\beta$ line-profile calculated data and to implement a combined technique of plasma density and temperature evaluation from the broadening and red-wing intensity of observable spectral feature (He$_\beta$ + $1snl3l' - 1s^2nl$} (Hammel *et al.*, 1994; Keane *et al.*, 1994b). For that purpose, detailed calculations of the relevant line profiles were done using the TOTAL (Calisti *et al.*, 1990) and MERL (Mancini *et al.*, 1991) codes. The calculations, however, show that these two codes provide somewhat different results while using the same atomic data. In this connection, a need for additional comparisons of calculated line profiles has been noted.

Figure 1 presents the line profiles of Ar He$_\beta$ in DD-plasma doped with Ar at the 0.1% atomic level at an electron density $N_e = 10^{24}$ cm^{-3} and temperature $T_e = T_i =$ 1 keV calculated using the HELM and LineDM codes in comparison with the TOTAL- and MERL-calculated data of Calisti *et al.* (1990) and Mancini *et al.* (1991). The comparison reveals the LineDM results practically coincident with the profile obtained using the MERL code (distinctions do not exceed 1–2%). On the other hand, the LineDM calculation considering the electron-collisional operator in the same manner as in the TOTAL model of Calisti *et al.* (1990), that is, with no factor of $\frac{1}{2}$ coming from the averaging over the Maxwellian velocity distribution (see above), has yielded a rather good agreement with the TOTAL-calculated profile. The remaining minor differences are likely to be caused by different models for calculating ion microfield distribution functions: TOTAL code uses the

https://doi.org/10.1017/S0263034600182175 Published online by Cambridge University Press

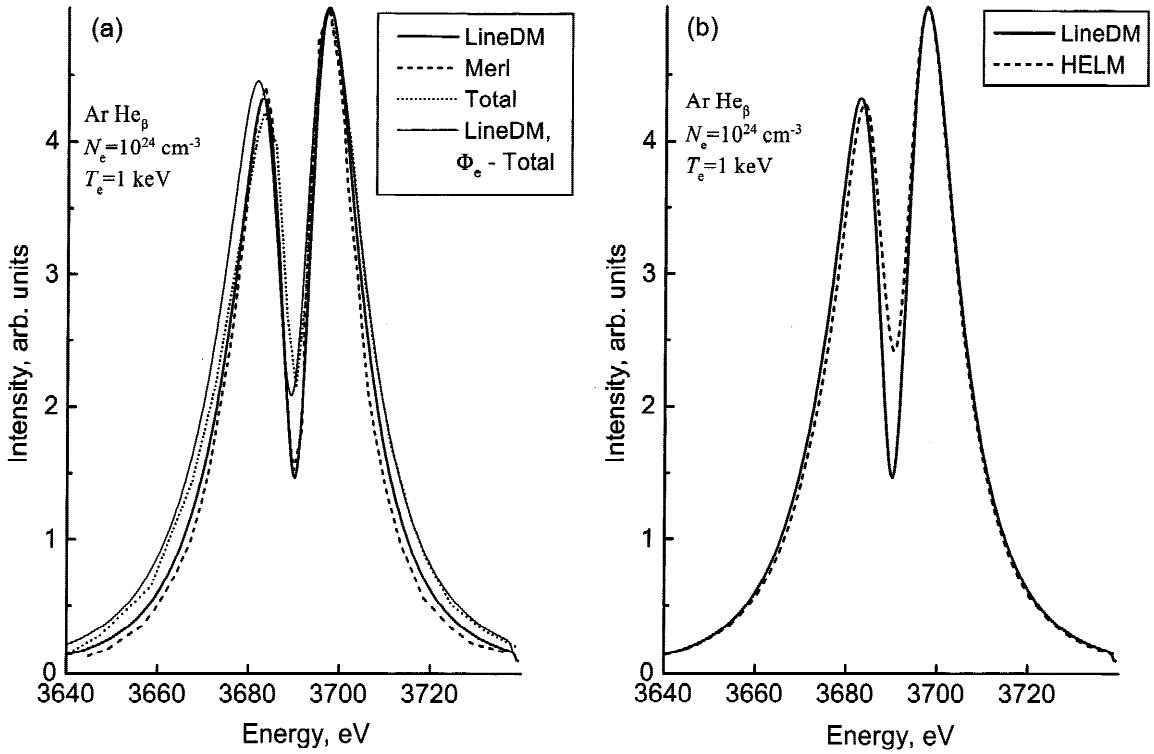

Fig. 1. Line profiles of Ar He_β calculated at plasma conditions typical for the NOVA-laser experiments of Hammel *et al.* (1994) and Keane *et al.* (1994*b*) with indirectly driven DD capsules. Solid and dotted lines represent the LineDM and TOTAL results, respectively. Dashed lines display the profile calculated with the MERL (a) and HELM (b) codes. Thin solid line represents the LineDM-calculated profile considering the electron-collisional operator in the same manner as in the TOTAL model of Calisti *et al.* (1990).

APEX model of Iglesias *et al.* (1983) while MERL and LineDM both utilize the variants of Hooper distribution (Tighe & Hooper, 1977). Therefore, our calculations allow us to suggest that the differences between the results provided by the TOTAL and MERL codes are attributed to the different models employed to calculate ion microfield distribution functions as well as to overestimated contribution of electron broadening in the TOTAL model. It can also be seen from Figure 1b that the calculation done with the HELM code yields practically the same result for the FWHM linewidth as both the LineDM and MERL codes do, but provides somewhat smaller depth of the central dip. The reason is that the HELM code considers only diagonal elements of relaxation operator $R^{\alpha\beta}_{\alpha\beta}$ in the Stark-state basis set (Loboda & Popova, 1997), or isolated Stark components approximation, and this is consistent with the results obtained by Calisti *et al.* (1990) and Keane *et al.* (1994*b*) also using the diagonal approximation for the elements of relaxation operator.

The line profile calculations of the satellite transitions $1s2l3l' - 1s^22l$ in Li-like Ar, performed by using the LineDM computer package for the same conditions, showed, that our results also yielded very good agreement with the MERL-calculated profile also being inconsistent with the TOTAL-code calculations of Keane *et al.* (1994*b*) in this case (see Fig. 2a). The agreement revealed is rather important, because this calculation is much more complicated than the previous one for the He_β line: here the sets $\{\alpha\}$ and $\{\beta\}$ respectively comprise 66 upper and 3 lower levels with $J_\beta = \frac{1}{2}, \frac{3}{2}$ (against 10 upper and 1 lower levels with $J_\beta = 0$ He_β has) thus essentially increasing the rank of coefficient matrix in the equation for the elements $\rho^q_{\alpha\beta}(\omega)$. We also note that in this case, the profile calculated under the diagonal approximation for the elements of relaxation operator, that significantly simplifies the calculations, differs by only within 4% from the line profile obtained in the full-scale mode and presented in Figure 2.

Contrary to the K_α-satellites $1s2l2l' - 1s^22l$ to the He_α line of Ar XVII (Woltz *et al.*, 1991), the profiles of the $1s2l3l' - 1s^22l$ satellite lines of interest are much more susceptible to the ion microfield effect. As one can see from Fig. 2b, the line profile calculated with the account of quasi-static ion broadening (Stark profile), is 2.5 times broader then the Voigt profile, employing only Doppler and relaxation (that is, homogeneous) broadening. Thus, for the appropriate numerical modeling of the experimental spectra near the He_β line at a temperature $T \leq 1$ keV, ion Stark broadening should be included for all the lines comprising the observed spectral feature $\{He_\beta + 1snl3l' - 1s^2nl\}$.

It is worth noting that consistent calculations of such net profiles should generally involve microfield-induced kinetic effect on the populations of autoionizing $1snl3l'$ levels:

https://doi.org/10.1017/S0263034600182175 Published online by Cambridge University Press

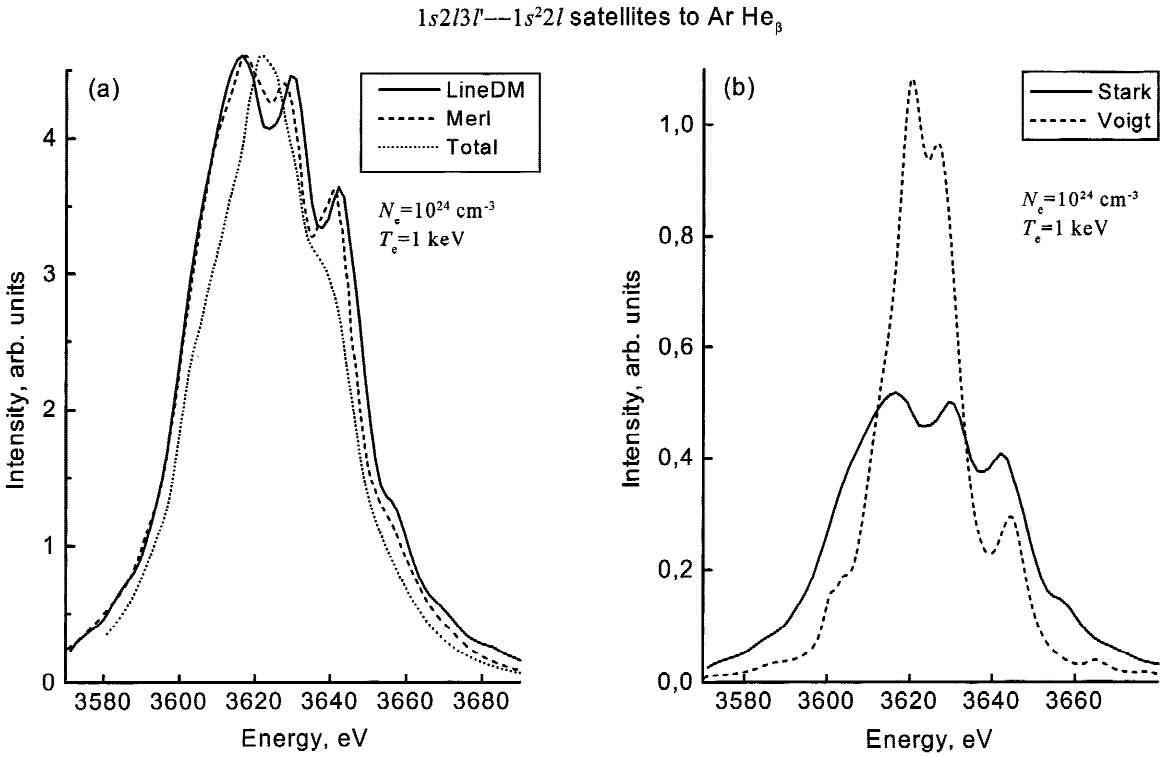

Fig. 2. Line profiles for the $1s2l3l' - 1s^22l$ transitions of Ar XVI, calculated at plasma conditions typical for the NOVA-laser experiments of Hammel *et al.* (1994) and Keane *et al.* (1994b) and the LTE distribution of the $1s2l3l'$-state populations. Solid and dotted lines represent the LineDM and TOTAL results, respectively. In the left subplot (a), dashed line displays the MERL-calculated profile, while in the right one (b) it shows the profile calculated with the LineDM code without the inclusion of ion Stark broadening (Voigt profile).

Stark mixing of the relevant states with different parities can essentially stimulate the processes of resonant (non-radiative) capture of electrons at these levels (Woltz *et al.*, 1991). Theoretical model implemented in the LineDM package is reasonably suitable for solving this problem and later on we are planning to perform such calculations to analyze the emission spectra of ultrashort-pulse-driven plasmas, where these effects may appear to be even more significant (Osterheld, 1998).

Using the LineDM package, a set of line-profile calculations have been performed for the $n = 5, 6$ to 1 resonant lines of He-like Al in Al plasmas at electron densities $N_e = 10^{20}$–10^{22} cm^{-3} and temperatures $T_e = 50$–250 eV. The calculated data were fitted to the relevant high-resolution experimental spectra of Stepanov *et al.* (1998) and Faenov (1998), registered with spherically bent mica crystal spectrometer. These fittings enabled us to evaluate effective values of plasma temperature and density at different distances from the surface of Al target driven by a XeCl-laser pulse (Faenov *et al.*, 1996).

The profile-fitting procedure was done by using a special-purpose module of the LineDM package mentioned above and its result is exemplified in Figure 3a,b. The values of electron density N_e and temperature $T_e = T_i$ given in the plots provide the best agreement of calculated profiles to the relevant experimental spectra recorded at a close distance $x < d_f$ (d_f is the focal spot diameter) from the target surface. From Figure 3 we notice that the fittings of the $n = 5$ to 1 (a) and $n = 6$ to 1 (b) lines yield rather close electron densities $N_e = 1.9 \times 10^{21}$ cm^{-3} and 1.5×10^{21} cm^{-3}, respectively, while the relevant temperatures differ as much as nearly twice. The latter difference should, nevertheless, be considered as a reasonable one, because the net temperature sensitivity of the central-feature line profiles, like that of the $n = 6$ to 1 line, is somewhat blurred. The reason is that the electron collisional broadening strongly affects the central features of these lines, while its temperature variations have an opposite impact on the line profiles, compared to Doppler and ion Stark broadening.

Moreover, such a comparison of the calculated and experimental spectra at a certain distance from target surface actually yields just some effective values of plasma electron density and temperature. These values correspond to the time- and space (resolved plasma layer)-integrated spectra allowing for the actual spatial resolution and instrumental function of the spectrometer. In fact, for every distance of registration, the emission in these lines is recorded at different instants of time from the spatial points with different plasma densities and temperatures. For this reason, realistic local density and temperature values of the ex-

https://doi.org/10.1017/S0263034600182175 Published online by Cambridge University Press

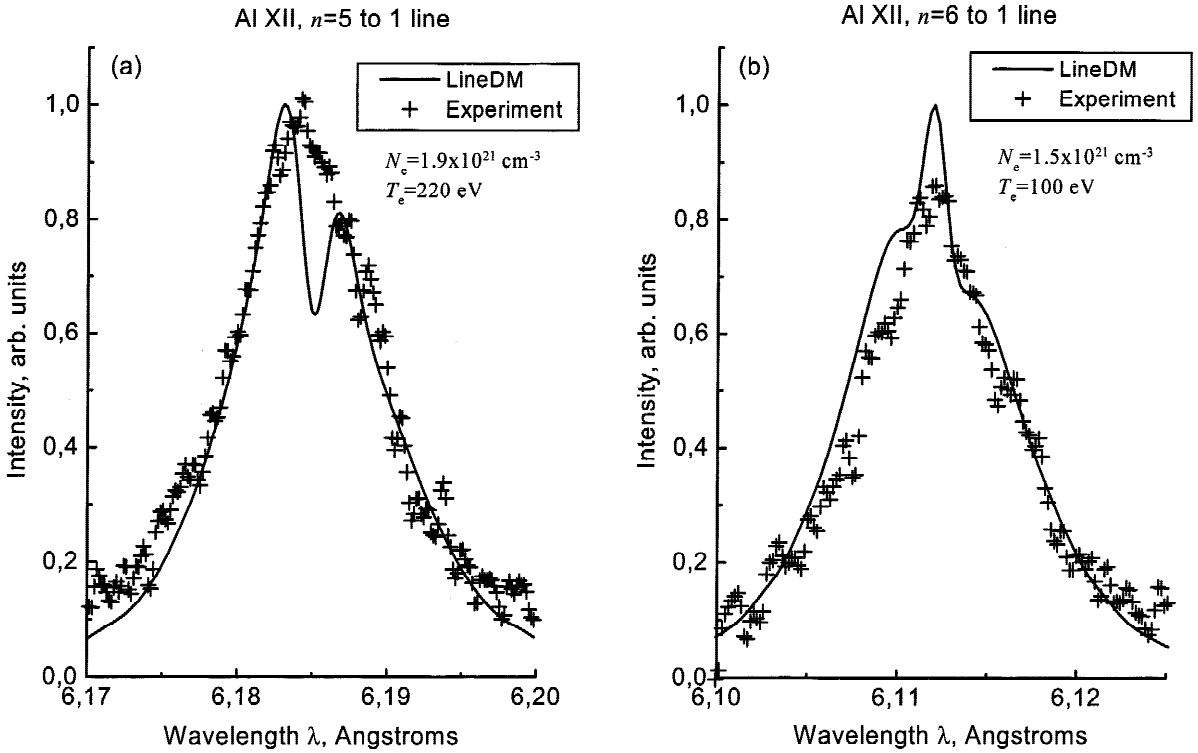

Fig. 3. Profiles of the $n = 5$ to 1(a) and $n = 6$ to 1(b) resonance lines of AI XII at a close distance $x \approx 30\ \mu\text{m} < d_f$ (d_f is the focal spot diameter) from the target surface. Solid curves represent LineDM-calculated profiles, while the pluses correspond to the experimental data of Stepanov *et al.* (1998) and Faenov (1998). The values of electron density N_e and temperature $T_e = T_i$ providing the best agreement of calculated and experimental data are given in the plots.

panding Al plasma can be retrieved only by solving an inverse problem of numerical reconstruction of registered spectra accounting for the actual experimental setup. This modeling would involve detailed radiative hydrodynamics of the Al-plasma coupled with the ionization and population kinetics of ionic states with follow-on calculation of time- and observation-plane-integrated Stark broadened profiles convolved with the instrumental function of spectrometer.

In the future, we plan to perform the numerical reconstruction of the Al XII $n = 5$, 6 to 1 line radiation spectra of Faenov (1998) at various distances from the Al-target surface to evaluate the inaccuracies introduced by using the local Stark-broadened line-profile data to immediately retrieve the spatial distribution of average electron densities and temperatures of expanding laser-produced plasmas.

The use of the *L*-shell spectra from the elements with high $Z \sim 50$ for diagnosing ICF capsules has some advantages compared to the *K*-shell spectra from the elements with lower $Z \sim 15$–20 since the optically thick pusher regions are more transparent for higher energy *L*-shell photons. This appears to be especially important in the investigations of high-performance targets utilizing laser-pulse shaping technique to provide lower-isentrope compression of the DD or DT fuel (Hammel *et al.*, 1994). In these targets, the increased pusher opacity in the range of the *K*-shell emission photons from the elements with $Z \leq 20$ does not affect the higher energy *L*-shell spectra. Specifically, diagnostic properties of the *L*-shell emission spectra in the wavelength range $\lambda \cong$ 2–3 Å were investigated in the indirectly driven ICF implosions on the NOVA laser (Hammel *et al.*, 1994; Keane *et al.*, 1994*b*) for the $2p^5 3d - 2p^6$, $2p^5 4d - 2p^6$, $2l^{-1}3l3l' - 2p^5 3l$ transitions of Ne-like and Na-like Xe and I, doped to the target DD-fuel and shell regions, respectively. Here, the intensity ratios of the spectral features referred to the groups of resonance (Ne-like) and relevant satellite (Na-like) transitions were found to exhibit a pronounced sensitivity both to electron temperature and density.

In this connection, the detailed study of *L*-shell transition spectra from Ne-like and Na-like emitters in laser-produced plasma is of particular interest for the development of promising methods of the ICF-target plasma diagnostics.

Figures 4 and 5 present the line profiles for the $2p^5 4l - 2p^6$ resonance transitions of Ne-like Cu calculated at an electron densities $N_e = 10^{22}$,10^{23} cm^{-3} of Cu plasma. Detailed experimental studies of these transition spectra were previously performed on the Hercules XeCl laser facility (ENEA, Frascati) by Bollanti *et al.* (1995) at typical plasma densities $N_e = 10^{22}$ cm^{-3} to test the diagnostic methods for the NOVA-laser experiments.

Figure 4 shows that at the density $N_e = 10^{22}$ cm^{-3} the interaction with plasma ion microfield gives rise to the well-

https://doi.org/10.1017/S0263034600182175 Published online by Cambridge University Press

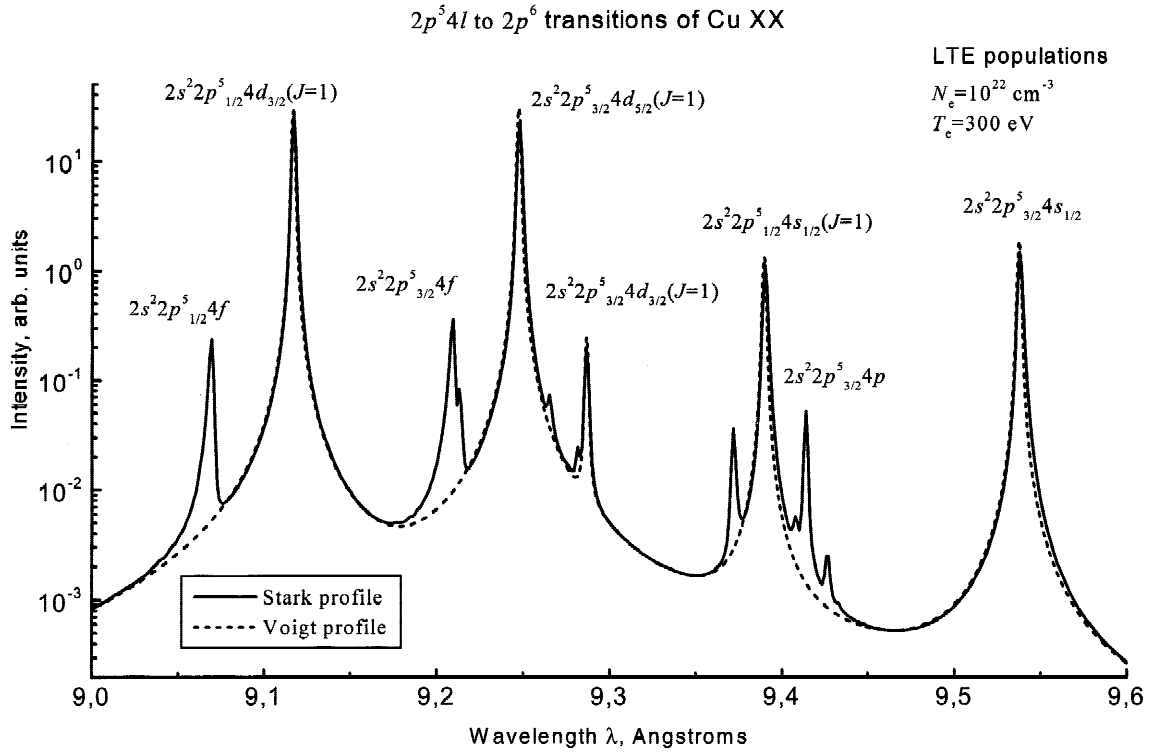

Fig. 4. Line profiles for the $2p^5 4l$–$2p^6$ resonance transitions of Ne-like Cu calculated at an electron density $N_e = 10^{22}$ cm^{-3} of Cu plasma. Solid and dashed curves represent the profiles obtained with and without the inclusion of ion Stark broadening, respectively.

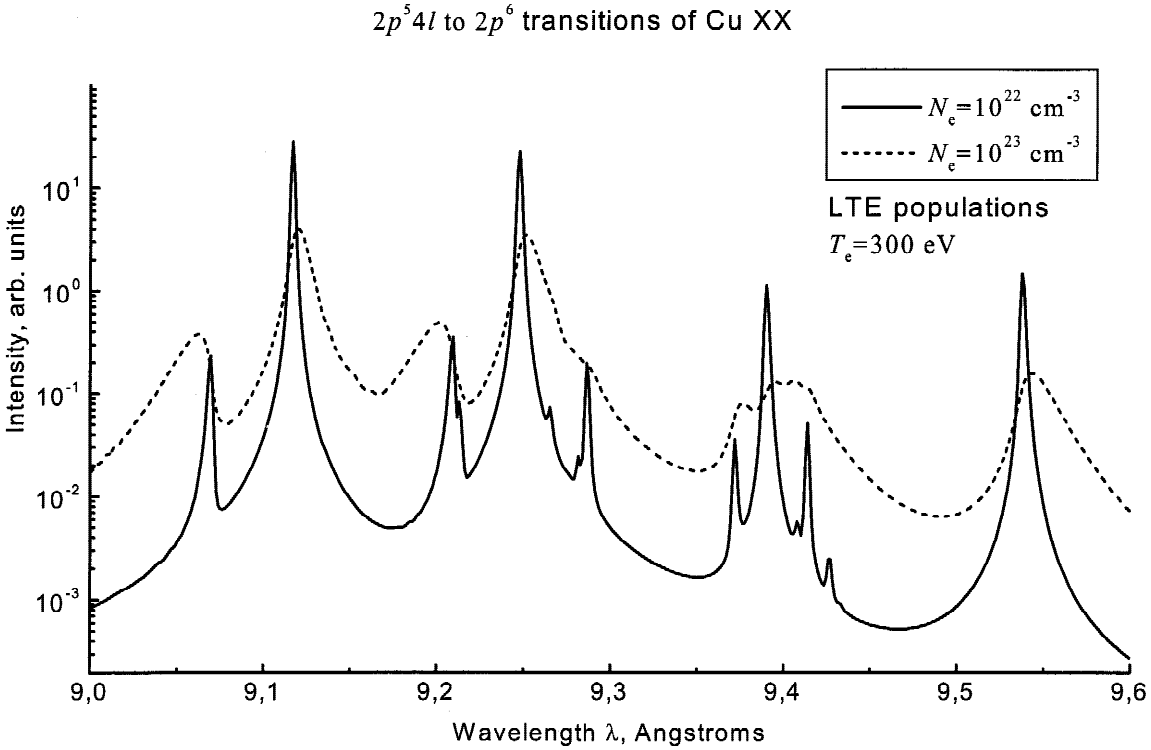

Fig. 5. Line profiles for the $2p^5 4l$–$2p^6$ resonance transitions of Ne-like Cu calculated at the Cu-plasma electron densities $N_e = 10^{22}$, 10^{23} cm^{-3}.

https://doi.org/10.1017/S0263034600182175 Published online by Cambridge University Press

pronounced forbidden components in the spectra of the $2p^5 4d$–$2p^6$ transitions, though their intensities are small enough for the experimental registration.

However, a tenfold increase of plasma density (Fig. 5) results not only in significant broadening of all spectral features in the wavelength range λ = 9–9.6 Å, but also in much the same, tenfold, lowering of the intensity ratios of the allowed $[2p^5_{1/2}4d_{3/2}(J=1) - 2p^6, 2p^5_{3/2}4d_{5/2}(J=1) - 2p^6]$ to forbidden $(2p^5_{1/2}4f - 2p^6, 2p^5_{3/2}4f - 2p^6)$ components near 9.07 and 9.12, 9.21, and 9.25 Å. So, this may well serve as a rather sensitive tool of plasma density evaluation.

Figures 6 and 7 present line profiles for the $2l^{-1}4l'$–$2p^6$ resonance transitions of Ne-like Xe calculated at Xe-plasma electron densities $N_e = 10^{23} - 5 \times 10^{24}$ cm^{-3}. The emission spectra from the Xe-filled capsule were investigated in the NOVA-laser experiments aimed at the development of the relevant L-shell X-ray diagnostics for the future experiments with indirectly driven capsules on the NIF facility (Osterheld, 1998).

Figure 6 shows, that at the lower electron density considered, $N_e = 10^{23}$ cm^{-3}, forbidden components of the Xe XLV $2p^5 4d$–$2p^6$ transition spectra are more abundant, than for Cu XX (Fig. 4). This is due to much greater energy splitting of the $2p^5 4l$ levels of Xe XLV and, consequently, to better resolution of the $n = 4$ to 2 line components of Xe XLV.

As the density increases to $N_e = 10^{24}$ cm^{-3}, the ratios of the allowed-to-forbidden spectral feature intensities at the wavelengths λ = 1.9, 1.99, 2.09 Å, and 2.12–2.15 Å get substantially lower up to 1–10, thus enabling to implement the relevant plasma density diagnostics in the laser-target experiments with anticipated values of $N_e \geq 10^{24}$ cm^{-3}.

We also note that with the Xe gas doped to the DD or DT-filled capsules at approximately 0.02% atomic level (Hammel *et al.*, 1994), the average Holtzmark field due to plasma ions appears to be only trice as lower as in the case of pure Xe filler at the same value of electron density N_e. Therefore, keeping in mind the difficulties of retrieving plasma densities through the linewidths of the $2p^5 4d$–$2p^6$ lines due to their minor values (<10 eV) at $N_e \leq 10^{25}$ cm^{-3}, plasma density evaluation from the ratios of the allowed-to-forbidden spectral feature intensities seems to be even more preferable. One can see from Figure 7 that the components $2s4p(J=1) - 2p^6$ and $2s4d - 2p^6$, $2p^5_{1/2}4d_{3/2}(J=1) - 2p^6$ and $2p^5_{1/2}4f - 2p^6$, $2p^5_{3/2}4d_{5/2}(J=1) - 2p^6$ and $2p^5_{3/2}4f - 2p^6$ are well-resolved and have comparable intensities at $N_e > 10^{24}$ cm^{-3} and thus are well suitable for diagnostic use.

6. CONCLUSION

We have described a theoretical model utilizing the density-matrix formalism to calculate spectral line profiles of arbitrary multielectron ions in plasmas. Line-profile calculation involves electron collisional and radiative relaxation of ionic states, emitter's motion (Doppler effect) and its interaction with quasi-static ion microfield. This model resulted from

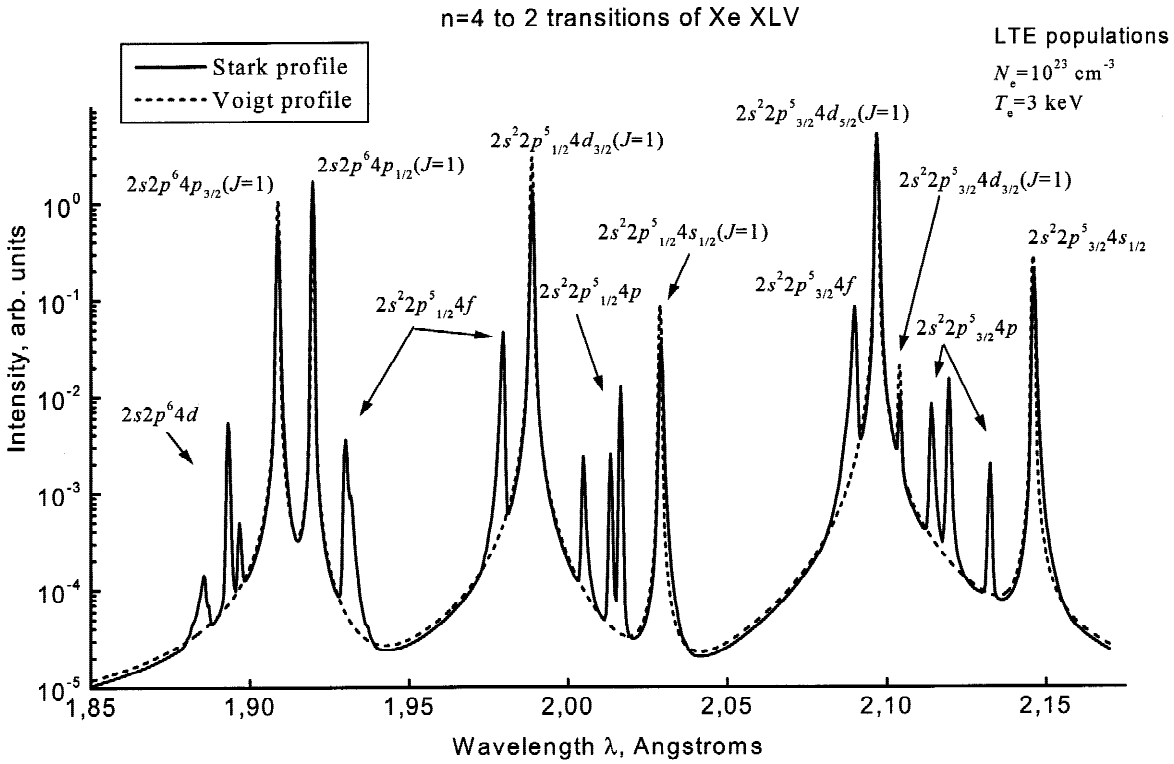

Fig. 6. Line profiles near $2l^{-1}4l'$–$2p^6$ resonant transitions of Xe XLV, calculated for Xe-plasma density $N_e = 10^{23}$ cm^{-3} with and without ion Stark broadening.

https://doi.org/10.1017/S0263034600182175 Published online by Cambridge University Press

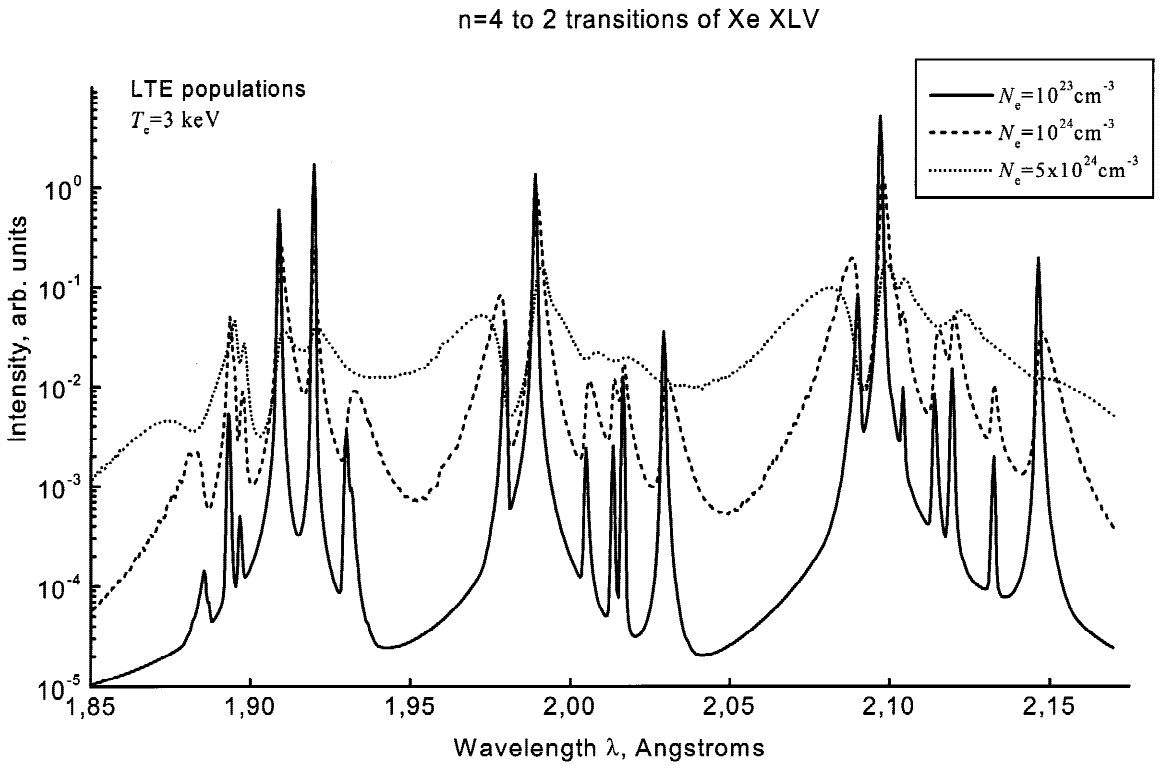

Fig. 7. Line profiles for the $2l^{-1}4l'$–$2p^6$ resonance transitions of Ne-like Xe calculated at Xe-plasma electron densities $N_e = 10^{23}$, 10^{24}, 5×10^{24} cm^{-3}.

the extension of the previously developed simplified model for calculating spectral line and gain profiles for the lines of simple ions implemented in the HELM code (Loboda *et al.*, 1992, 1997; Loboda & Propova, 1997), and is generally free of limitations set by the approximations of the previous model. In particular, the sets of the upper or lower states involved in the transitions of interest, are not fixed but formed in every specific case depending on the frequency interval and plasma density considered. The diagonal approximation for density-matrix elements and the isolated Stark components approximation are generally not adopted, but may be used in particular cases.

Using the LineDM computer package implementing this model, line-profile calculations of the *K*- and *L*-shell transitions in Al XII, Ar XVII, Ar XVI, Cu XX, and Xe XLV ions have been performed in the context of plasma diagnostic issues of some recent laboratory experiments. Comparisons of the modeled line profiles with the experimental and other theoretical data show the applicability of the model implemented in the LineDM computer package for the analysis of X-ray line radiation spectra from multielectron emitters in hot dense plasmas.

ACKNOWLEDGMENTS

The authors are grateful to our colleagues Drs. A.Ya. Faenov, I.Yu. Skobelev, and A.L. Osterheld for their continuing interest to these activities, for stimulative discussions, and providing the necessary experimental data. The authors would also like to thank Prof. I.P. Grant for providing the up-to-date version of the GRASP[2] code. This work has been supported in part by the ISTC Projects. #076 and 525.

REFERENCES

Akhmedov, E.Kh. *et al.* (1985). *Zh. Eksp. Teor. Fiz. (Sov. Phys.: JETP)* **89**, 470.

Anufrienko, A.V. *et al.* (1990). *Zh. Eksp. Teor. Fiz. (Sov. Phys.: JETP)* **98**, 1304.

Anufrienko, A.V. *et al.* (1993). *Zh. Eksp. Teor. Fiz. (Sov. Phys.: JETP)* **103**, 417.

Baranger, M. (1962). In *Atomic and Molecular Processes* (D.R. Bates, ed.), ch. 13 (N.Y.: Academic Press).

Blum, K. (1981). *Density Matrix Theory and Applications* (N.Y. & London: Plenum).

Bollanti, S. *et al.* (1995). *Physica Sripta* **51**, 326.

Calisti, A., Khelfaoui, F., Stamm, R., Talin, B. & Lee, R.W. (1990). *Phys. Rev. A.*, **42**, 5433.

Calisti, A., Godbert, L., Stamm, R. & Talin, B. (1994). *J. Quant. Spectrosc. Radiat. Transfer* **51**, 59.

Cooper, J. (1967). *Rev. Mod. Phys.* **39**, 167.

Cowan, R.D. (1981). *The Theory of Atomic Structure and Spectra* (Berkeley, L.A., London: U.C. Press).

Derzhiev, V.I., Zhidkov, A.G. & Yakovlenko, S.I. (1986). *Radiation of Ions in Nonequilibrium Dense Plasmas* (Moscow: Energoatomizdat) [in Russian].

Dyall, K.G., Grant, I.P., Johnson, C.T., Parpia, F.A. & Plummer, E.P. (1989). *Comput. Phys. Commun.* **55**, 425.

https://doi.org/10.1017/S0263034600182175 Published online by Cambridge University Press

Elton, R.C. (1990). *X-ray Lasers* (San-Diego: Academic Press Inc.).
Elton, R.C. *et al.* (1997). *J. Quant. Spectrosc. Radiat. Transfer* **58**, 559.
Faenov, A.Ya. *et al.* (1996). *Kvant. Elektron. (Sov. Phys. Quantum Electronics)* **23**, 719.
Faenov, A.Ya. (1998). *Private communication.*
Froese Fischer, C. (1978). Comput. Phys. Commun. **14**, 145.
Gasparyan, P.D., Gerasimov, V.M., Starostin, A.N. & Suvorov, A.E. (1994). *Zh. Eksp. Teor. Fiz. (Sov. Phys. JETP)* **105**, 1593.
Griem, H.R. (1974). *Spectral Line Broadening by Plasmas* (N.Y. & London: Academic Press).
Griem, H.R. (1986). *Phys. Rev. A* **33**, 3580.
Griem, H.R., Blaha, M., Kepple, P.C. (1979). *Phys. Rev. A* **19**, 2421.
Hammel, B.A. *et al.* (1994). *J. Quant. Spectrosc. Radiat. Transfer* **51**, 113.
Hauer, A. (1981). In *Spectral Line Shapes*, Vol. 1 (B. Wende, ed.), p. 295 (Berlin: W. de Gruyter & Co).
Iglesias, C.A., Lebowitz, J.L. & MacGowen, D. (1983). *Phys. Rev. A.* **28**, 1667.
Iglesias, C.A., Rogers, F.J. & Wilson, B.G. (1987). *Astrophys. J. Lett.* **322**, L45.
Karazija, R. (1987). *Introduction to the theory of X-ray and electron spectra of free atoms.* (Vilnius: Mokslas) [in Russian].
Keane, C.J. *et al.* (1994a). *Phys. Rev. Lett.* **72**, 3029.
Keane, C.J. *et al.* (1994b). *J. Quant. Spectrosc. Radiat. Transfer* **51**, 147.
Kepple, P.C. & Griem, H.R. (1968). *Phys. Rev.* **173**, 317.
Loboda, P.A., Lykov, V.A. & Popova, V.V. (1992). *Proc. SPIE* **1928**, 145.
Loboda, P.A., Lykov, V.A. & Popova, V.V. (1993). *Proc. SPIE* **2012**, 232.
Loboda, P.A. & Popova, V.V. (1997). *RFNC VNITF Preprint* No. 63. [in Russian].
Loboda, P.A., Popova, V.V. & Shinkarev, M.K. (1997). *J. Quant. Spectrosc. Radiat. Transfer* **58**, 757.
Lykov, V.A., Avrorin, E.N., Loboda, P.A., Politov, V.Yu. (1992). In *X-ray lasers*, IOP Conf. Ser. **125** (E.E. Fill, ed.), p. 155 (Bristol, England: IOP Publishing Ltd.).
Mancini, R.C., Kilkrease, D.P., Woltz, L.A. & Hooper, Jr., C.F. (1991). *Comput. Phys. Commun.* **63**, 314.
Mancini, R.C., Hooper, Jr., C.F. & Coldwell, R.L. (1994). *J. Quant. Spectrosc. Radiat. Transfer* **51**, 201.
Mancini, R.C. *et al.* (1996). *Phys. Rev. E* **54**, 4147.
Mewe, R. (1972). *Astron. Astrophys.* **20**, 215.
Mollow, B.R. & Miller, M.M. (1969). *Ann. of Phys.* **52**, 464.
Mollow, B.R. (1977). *Phys. Rev. A* **15**, 1023.
Moreno, J.C., Griem, H.R. & Goldsmith, S. (1989). *Phys. Rev. A.* **39**, 6033.
Moreno, J.C., Griem, H.R., Lee, R.W. & Seely, J.F. (1993). *Phys. Rev. A* **45**, 374.
Olson, G.L., Comly, J.C., La Gattuta, J.K. & Kilcrease, D.P. (1994). *J. Quant. Spectrosc. Radiat. Transfer* **51**, 255.
Osterheld, A.L. (1997). *Private Communication.*
Osterheld, A.L. (1998). *High Energy Density Physics Research in the LLNL High Temperature Physics Division*, 5th Zababakhin Scientific Talks (Snezhinsk, Russia).
Parpia, F.A., Grant, I.P. & Fischer, C.F. (1992). *GRASP[2] user's reference* (unpublished).
Parpia, F.A., Fischer, C.F. & Grant, I.P. (1996). *Comput. Phys. Commun.* **94**, 249.
Politov, V.Yu., Lykov, V.A. & Shinkarev, M.K. (1992). *Proc. SPIE* **1928**, 157.
Rautian, S.G., Smirnov, G.I. & Shalagin, A.M. (1979). *Nonlinear Resonances in Atomic and Molecular Spectra* (Nauka, Novosibirsk) [in Russian].
Rosmej, F.B. *et al.* (1997). *J. Quant. Spectrosc. Radiat. Transfer* **58**, 859.
Skobelev, I.Yu. *et al.* (1995). *Zh. Eksp. Teor. Fiz. (Sov. Phys. JETP)* **108**, 1263.
Smith, E.W. & Hooper, Jr., C.F. (1967). *Phys. Rev.* **157**, 126.
Stamm, R., Talin, B., Pollock, E.L. & Iglesias, C.A. (1987). In *Spectral Line Shapes*, Vol. 4 (R.J. Exton, ed.), p. 141 (Hampton, VA: A. Deepak Publ.).
Stepanov, A.E. *et al.* (1998). *Modeling of the Spectral Lines Radiation in laser-produced plasmas expanding in He gas with atmospheric pressure*, In Abstr. 25th ECLIM (Formia, Italy).
Tighe, R.J. & Hooper, Jr., C.F. (1977). *Phys. Rev. A* **15**, 1773.
Vainshtein, L.A., Sobel'man, I.I. & Jukov, E.A. (1981). *Excitation of atoms and broadening of spectral lines* (Springer-Verlag, Berlin).
Van Regemorter, R. (1962). *Astrophys. J.* **132**, 906.
Woltz, L.A. & Hooper, Jr., C.F. (1988). *Phys. Rev. A* **38**, 4766.
Woltz, L.A., Jacobs, V.L., Hooper, Jr., C.F. & Mancini, R.C. (1991). *Phys. Rev. A* **44**, 1281.
Yaakobi, B. *et al.* (1979). *Phys. Rev. A* **19**, 1247.
Zhidkov, A.G., Tkachev, A.N. & Yakovlenko, S.I. (1986). In *The Processes in the Inner Atomic Shells* (Council for Spectroscopy of the USSR Academy of Sciences, Moscow), p. 5. [in Russian].
Zhidkov, A.G. & Yakovlenko, S.I. (1985). *General Physics Institute Preprint No. 246* (Moscow). [in Russian].
Zygelman, B. & Dalgarno, A. (1987). *Phys. Rev. A* **35**, 4085.

Appendix

Since the main contribution to $R_c^{(1)}$ is usually provided by the collisions with sufficiently large values of electron angular momenta, function G can be correctly evaluated to the second-order expansion terms of electron-ion interaction under the classical-path assumption for the perturbing electron. Evaluations of this type were commonly used for electron impact broadening calculations. Generally, straight classical path approximation was employed and the averaging over the Maxwell distribution of electron velocities was performed either approximately (Griem, 1974; Anufrienko *et al.*, 1993; Loboda & Popova, 1997) or with a fixed value of minimum impact parameter $b_{\min}$ chosen equal to the radius of outermost Bohr orbit of the excited electron, (Griem *et al.*, 1979; Calisti *et al.*, 1990; Loboda & Popova, 1997), $a_n \simeq n^2 a_0/z$ (n is the principal quantum number of the excited electron, z is the spectroscopic symbol of the emitter, approximately denoting the effective charge of the ionic core).

However, using the straight-classical-path assumption, one can obtain a general expression for the G-function free of these simplifications and accounting for the dependence of

https://doi.org/10.1017/S0263034600182175 Published online by Cambridge University Press

maximum and minimum impact parameters ratio in the Coulomb logarithm on the electron velocity:

$$\ln\left(\frac{b_{\max}(v)}{b_{\min}(v)}\right) = f(v).$$

Skipping the derivation details and estimating a contribution due to strong collisions with impact parameters $b \le b_{\min}$ similar to Kepple & Griem (1968), we write the final expression:

$$G^{pq}_{ijk(l)} = \frac{1}{2}\,\mathrm{Ei}(-y_1^*) + \frac{1}{2}\,\mathrm{Ei}(-y_2^*) - \frac{3}{2}\,\mathrm{Ei}(-y_{\min}) + \frac{\pi}{6}\,y_{\min} \tag{A1}$$

where; $\mathrm{Ei}(x)$ is the integral exponential function, and parameters $y_1^*, y_2^*, y_{\min}$ are defined as follows:

$$y_1^* = \max\{y_{\min}, y_3\};\ y_2^* = \max\{y_{\min}, y_2\};$$

$$y_{\min} = \max\left\{[(y_1')^2 y_3']^{1/3}, y_1', \frac{(y_1')^2}{y_2'}\right\}$$

$$y_3 = \min\{(y_2' y_3')^{1/2}, y_3'\};\ y_2 = \max\{(y_2' y_3')^{1/2}, y_2'\}.$$

Here

$$y_1' = \frac{\chi\!\!\!^{-}_D(v_0)}{b^{ijk(l),pq}_{\max}(v_0)},\ y_2' = \left(\frac{\chi\!\!\!^{-}_D(v_0)}{a^{pq}_{n>}}\right)^2,\ y_3' = \left(\frac{L_c(v_0)}{\chi\!\!\!^{-}_D(v_0)}\right)^2,$$

$$b^{ijk(l),pq}_{\max}(v_0) = \frac{v_0}{(\tilde{\Gamma}^2_{pq} + \omega_p^2 + \omega^2_{ijk(l)>})^{1/2}}, \tag{A2}$$

where $L_c(v_0) = [(z-1)e^2]/mv_0^2$ is the Coulomb parameter of the perturbing electron at the average thermal velocity $v_0 = \sqrt{2T/m}$, $a^{pq}_{n>}$ is the Bohr radius of the excited state with $n_> = \max\{n_p, n_q\}$, and $\chi\!\!\!^{-}_D(v_0) = \hbar/mv_0$ is responsible for the de Broglie impact parameter cutoff, that is, for the limitation of classical description of the electron–ion collisions. The strong-collision (Weisskopf) cutoff for nonadiabatic electron broadening (Griem, 1974) in the cases when $E_{aa'}, E_{bb'} \ll E_{ab}, E_{a'b'}$ (the states a, a' and b, b' belong to the nonoverlapping sets of levels), was omitted: one can readily see that for high-Z ions with $z \ge 10$ in the cases of practical interest $b_s \le \chi\!\!\!^{-}_D$. Specifying the maximum impact parameter, finite value of the lifetime of the $p-q$ line components, represented by the total width $\tilde{\Gamma}_{pq} = \frac{1}{2}(\Gamma^r_p + \Gamma^r_q + \Gamma^{ci}_p + \Gamma^{ci}_q)$ was taken into account as well as the Debye screening and adiabatic cutoff, included through the electron plasma frequency ω_ρ and frequency interval between the closely-spaced states (Griem, 1974), respectively,

$$\omega_{ijk>} = \max\{|\omega_{ij}|, |\omega_{jk}|\},\ \omega_{ijkl>} = \max\{|\omega_{ik}|, |\omega_{jl}|\}.$$

If one lets that at all essential Maxwellian electron velocities v

$$b_{\min} = \max\{L_c(v), \chi\!\!\!^{-}_D(v), a_{n>}\} = a_{n>},$$

the function G (A1) takes the form:

$$G^{pq}_{ijk(l)} = -\frac{1}{2}\,\mathrm{Ei}(-y_{\min}) + \frac{\pi}{6}\,y_{\min},\ y_{\min} = \left(\frac{a^{pq}_{n>}}{b^{ijk(l),pq}_{\max}(v_0)}\right)^2. \tag{A3}$$

Equation (A3) is analogous to the expression for $G(\Delta\omega = 0)$ of Calisti *et al.* (1990) to an accuracy of the factor $\frac{1}{2}$ at the integral exponential function and substitution of the last term by the strong collision constant $C_{n>}$ (Griem *et al.*, 1979).

To examine the Eq. (A1), the relevant collisional rates $C_{b'a} = \langle v\sigma_{ab'}\rangle = (R_c)^{b'b'}_{aa}/N_e$ (8) of the electron impact transitions $b' = 2s_{1/2} \to a = 2p_{1/2}, 2p_{3/2}$ of H-like Ar XVIII were compared to the data calculated by Zygelman and Dalgarno (1987) using the close-coupling method, straight classic path assumption with $b_{\min} = a_{n>}$ (Griem *et al.*, 1979), and the approximation formulas of Van Regemorter (1962) and Mewe (1972) as well. At the temperatures $T \ge z^2\mathrm{Ry}/8$, typical for the laser-produced plasmas, our expression for transition rates was found to agree with the close-coupling calculated data much better (within 3–5%) than all the other results (from 25 up to 100%).

For the elements $R_c^{(2)}$ in Eq. (8), responsible for the substantially inelastic collisional transitions to the distant ionic states, G-function is specified by using the effective Gaunt-factor approach (Baranger, 1962):

$$G^{pq}_{ijk(l)} = \frac{\pi}{\sqrt{3}}\,g(y_{ij})$$

$$g(y_{ij}) = \bar{g}(|y_{ij}|)[1 + \theta(y_{ij})(\exp(-|y_{ij}|) - 1)],\ y_{ij} = \frac{E_{ij}}{T}, \tag{A4}$$

where the values $\bar{g}(|y_{ij}|)$ are found either from the quantum-mechanical calculations of collisional transition rates $C_{ij} = \langle v\sigma_{ij}\rangle$ or evaluated by using the approximation formulas of Van Regemorter (1962) and Mewe (1972).

https://doi.org/10.1017/S0263034600182175 Published online by Cambridge University Press